Seasonal Variations of Snow Depth on Mars

David E. Smith,[1]* **Maria T. Zuber,**[1,2] **Gregory A. Neumann**[1,2]

Using topography collected over one martian year from the Mars Orbiter Laser Altimeter on the Mars Global Surveyor (MGS) spacecraft, we have measured temporal changes in the elevation of the martian surface that correlate with the seasonal cycle of carbon dioxide exchange between the surface and atmosphere. The greatest elevation change (1.5 to 2 meters) occurs at high latitudes (above 80°), whereas the bulk of the mass exchange occurs at lower latitudes (below 75° N and below 73° S). An unexpected period of sublimation was observed during northern hemisphere autumn, coincident with dust storms in the southern hemisphere. Analysis of MGS Doppler tracking residuals revealed temporal variations in the flattening of Mars that correlate with elevation changes. The combined changes in gravity and elevation constrain the average density of seasonally deposited carbon dioxide to be 910 ± 230 kilograms per cubic meter, which is considerably denser than terrestrial snow.

Over the course of its year, Mars exchanges up to a third of its carbon dioxide (CO_2) atmosphere with the surface, resulting in a seasonal redistribution of about 50 billionths of the mass of the planet. The seasonal polar caps consist mainly of CO_2 frost deposits whose spatial and temporal distributions are controlled primarily by solar insolation (1). In the northern and southern hemispheres, CO_2 begins to condense out of the atmosphere at high latitudes during autumn as the surface encounters increasing darkness (Web fig. 1) (2), depositing a thin veneer of dry ice on the polar

caps and surroundings. Continued deposition causes the "frost line" to migrate from the polar regions toward the equator, and surface frost reaches mid-latitudes in late winter (3). In early spring, as the surface receives more sunlight, surficial CO_2 sublimates back into the atmosphere, causing the frost line to retreat to high latitudes.

The elevation of the north pole of Mars is 6 km lower than the south pole (4, 5). In the north during the summer, the temperature rises above the CO_2 condensation temperature, and dry ice frost deposited during the previous winter sublimes away, revealing a residual H_2O ice cap (6, 7). In contrast, the southern polar region is colder and has a lower atmospheric pressure, and as a consequence its surface veneer of CO_2 does not completely sublime. A residual dry ice surface is observed even in summer (8), although observations of atmospheric water vapor during some years (9, 10) have been cited

as evidence for at least some surficial H_2O (11). Both polar regions contain layered terrains that are characterized by about 3 km of relief (5, 12) and are believed to be composed primarily of H_2O ice mixed with dust. The residual north polar ice cap correlates well with elevated topography that defines the layered terrains (Fig. 1, left) (12). However, elevated layered deposits in the south are much broader in spatial extent than the residual ice cap (Fig. 1, right) (5).
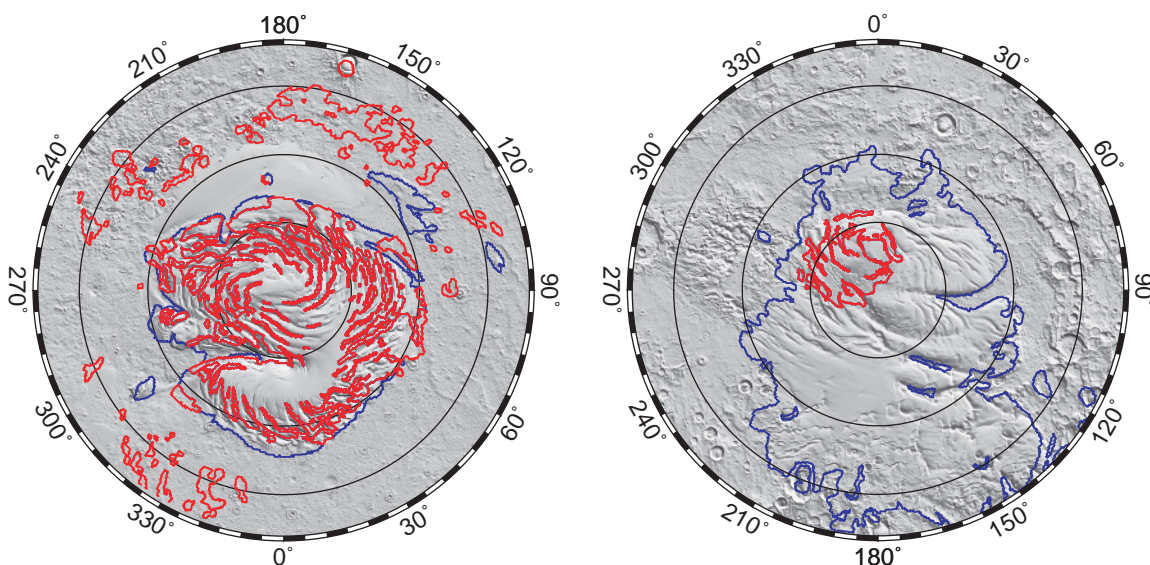
Using data from the Mars Orbiter Laser Altimeter (MOLA) (13) on the Mars Global Surveyor (MGS) (14) spacecraft, we have made the first measurements of temporal changes in the elevation of the surface of Mars and of the planet's global mass redistribution due to the yearly cycle of CO_2 exchange. We analyzed over 400 million elevation measurements (15) and over 66 million altimetric crossovers (16) from MOLA, as well as all MGS X-band Doppler and range tracking (17) observations collected during the MGS mapping and extended mission phases between 28 February 1999 and 25 May 2001 (18). The observations spanned more than a full martian year (19) and enabled us to observe the seasonal pattern repeating the early part of the cycle. In studying seasonal phenomena on Mars, it is customary to express time in terms of the solar longitude, L_s, which runs from 0° to 360° over one Mars year, and $L_s = 0$° is defined as the vernal equinox in the northern hemisphere. MGS began its global mapping mission at $L_s = 103$°, during northern hemisphere summer. Our analysis continued into the MGS extended mapping mission, through $L_s = 547$°. (We added 360° to L_s to denote observations collected during the second Mars year of mapping; for example, $L_s = 547$° is equivalent to $L_s = 187$°, which is northern fall.)

We analyzed MOLA profiles of elevation in over 1200 0.05°-wide (3 km-wide) latitu-

[1]Laboratory for Terrestrial Physics, NASA/Goddard Space Flight Center, Greenbelt, MD 20771, USA. [2]Massachusetts Institute of Technology, Cambridge, MA 02139–4307, USA.

*To whom correspondence should be addressed. E-mail: dsmith@tharsis.gsfc.nasa.gov

Fig. 1. Shaded relief maps of (**left**) north and (**right**) south polar topography of Mars. The projection is polar stereographic from latitude 72° to the poles. The red contours in each hemisphere represent the approximate extent of the residual ice caps (denoted by high albedo); the blue contours trace regions of elevated polar layered terrains.

dinal annuli between 60°–87°N, 60°–87°S and, to isolate systematic errors (20), in the equatorial band of 5°S to 5°N (21). Within each annulus, we created a longitude-averaged reference basal surface by fitting a 25-point running median to all points in all L_s bins in the annulus (Web fig. 2) (2). We then calculated residuals of individual elevations with respect to the basal topographic surface (Web fig. 3) (2, 22) and ordered the observations by the date on which they were collected. We averaged the residuals to the median surface in 15-day bins and removed a global systematic contribution to the elevation change by differencing the signal in each hemisphere to that at latitude 60° (20).

In a separate analysis of altimetric crossovers (16), we also divided the data into 15-day temporal bins, using only low-latitude (that is, non–temporally varying) crossovers and, to constrain short-period orbital errors, crossovers at higher latitudes within a given bin. As for the profile analysis, the crossover method used altimetry; however, this analysis was performed independently and provides a cross-check of the analysis of the profile data.

In order to minimize noise and maximize the signal, we averaged over longitude in both approaches to isolate zonal (latitudinal) variations (20). A formal error analysis yields a vertical accuracy in each 2-week bin of ± 5 to 6 cm (Table 1), whereas the observed bin-to-bin noise in the observations is ±10 cm (23).

In both hemispheres, the greatest high-latitude surface elevations were observed when the polar regions were in darkness, and the lowest elevations were observed when those areas were sunlit (Fig. 2). In both hemispheres, the maximum elevation occurred in late winter, and greater elevation changes were observed with increasing latitude. Because the pattern of changing elevation correlates approximately in both amplitude and phase (Web fig. 4) (2) with the expected signal of Mars' CO_2 cycle, and because errors do not exhibit the seasonal phase, we interpret the observed elevation changes as predominantly reflecting the seasonal cycle of CO_2 condensation and sublimation.

From the temporal pattern of elevation changes (Fig. 2 and Web movie 1) (2) we may track the seasonal behavior of CO_2 exchange. MGS began global mapping during northern hemisphere summer (Fig. 2, A and B), and all northern latitudes displayed minimum elevations. Just after the autumnal equinox ($L_s = 180°$), when high northern latitudes lost sunlight, CO_2 began to accumulate in greater amounts at progressively higher latitudes. However, in the period $L_s \sim$ 225° to 245°, the surface underwent rapid sublimation of up to 30 cm of material. This period of decreasing surface elevation is not predicted by the seasonal change in solar

insolation, but it does correlate with the occurrence of several regional dust storms (24). Although these dust storms were located mostly in the southern hemisphere, they raised the temperature of the atmosphere at mid- to high latitudes in the northern hemisphere by >20° (24). But a temperature increase of this magnitude alone cannot explain as much sublimation as was observed. Lateral atmospheric transport or redistribution of surface frost by wind (or both) are required to explain the magnitude of the off-season elevation decrease. Accumulation in the north resumed as the atmosphere cleared and cooled, and reached a longitudinally averaged maximum of ~1.5 m at 86.5°N at $L_s \sim$ 345°, during late winter (Table 1).

At the beginning of MGS mapping in the

southern hemisphere, the season was winter and CO_2 was accumulating at mid- to high southern latitudes (Fig. 2, C and D). The maximum accumulation in the south was achieved at $L_s \sim$ 155°, relatively earlier by 10° L_s than in the north. Sublimation in the southern hemisphere during spring may have been aided by atmospheric warming associated with dust storm activity discussed above. Substantial accumulation began again at about $L_s \sim$ 390°, in early southern fall.

In both hemispheres, the minimum zonal surface shows a variation of about 10 cm, which we interpret as a measure of our precision (Fig. 3). Both hemispheres show a quasi-linear latitudinal trend of maximum accumulation of about 4 cm per degree of latitude. In the south, the trend continued to the
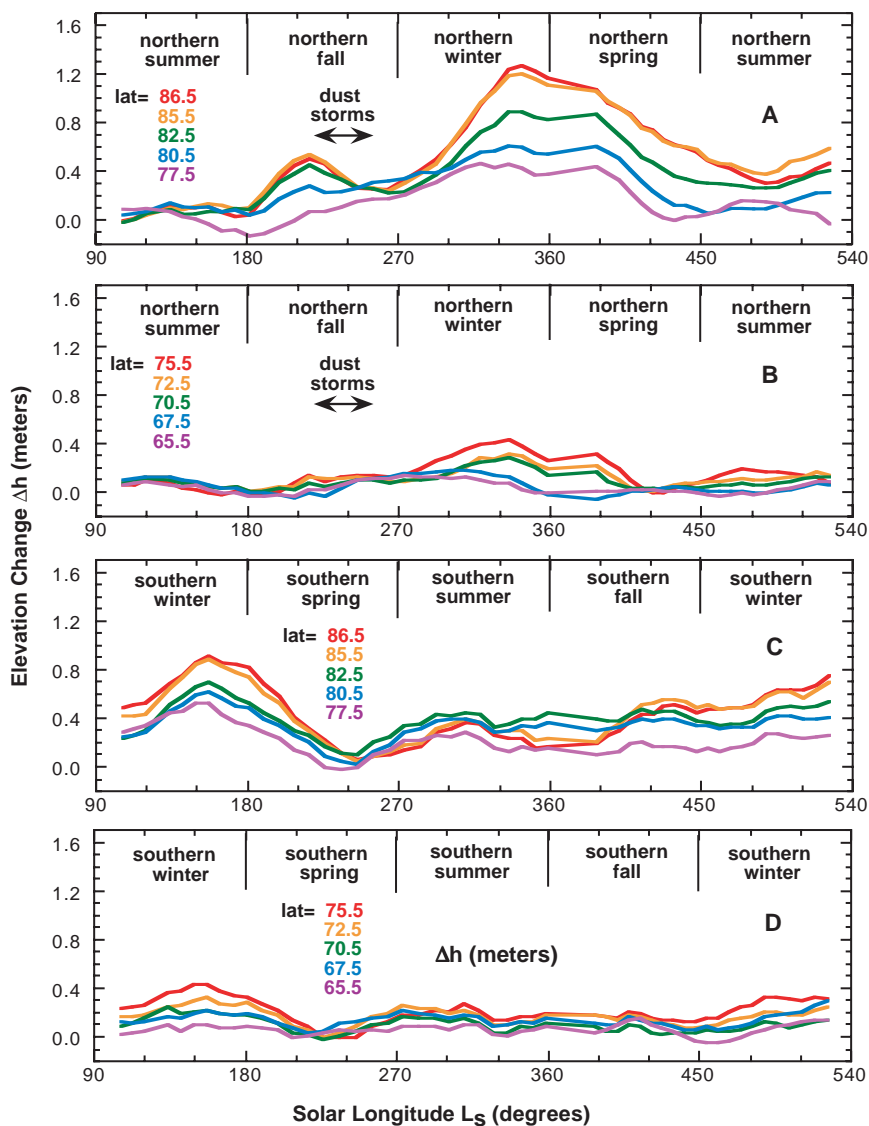
Fig. 2. Latitudinal profiles of elevation change (Δh) over the course of the MGS mapping mission and martian seasons (solar longitude L_s) in the (A) north polar, (B) north mid-latitude, (C) south polar, and (D) south mid-latitude regions. Shown in (A) and (B) is the time of regional dust storms (24) that warmed the atmosphere and caused off-season sublimation in the northern hemisphere. Elevation changes in the northern hemisphere are with respect to latitude 60°N and those in the southern hemisphere are with respect to 60°S.
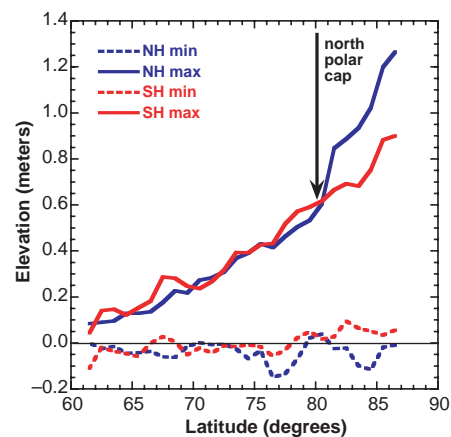
highest latitude sampled, whereas in the north the accumulation increased steeply on the residual ice cap to nearly 12 cm per degree of latitude. However, the greater deposition on the north polar cap did not contribute substantially to the total precipitated mass in the northern hemisphere, because of the small surface area over which it occurred. Greater accumulation on the ice cap as compared to that on surroundings is consistent with MOLA observations indicating the north polar cap to be a locus of atmospheric CO_2 condensation (*12, 25, 26*). The ice cap, with its higher albedo, is colder than its surroundings and spends more time below the CO_2 condensation temperature (*7*). It is likely that we were able to isolate the enhanced accumulation over the north polar cap in this zonal analysis because the cap is oriented approximately axisymmetrically about the north pole (Fig. 1A). Our approach cannot resolve whether the asymmetric south residual cap (Fig. 1B) also exhibited greater accumulation than its surroundings. The similarity in the latitudinal distribution of off-cap accumulation with latitude in the northern and southern hemispheres is surprising given the different elevations and thus near-surface temperatures. General circulation models (GCMs) of the martian atmosphere (*27*) predict similar maximum CO_2 ice accumulations but show ~35% more condensed mass in the southern hemisphere than in the north because of the longer southern fall and winter seasons.

As the martian year progressed, the latitudinal pattern of CO_2 showed alternating accumulation and sublimation at northern and southern high latitudes. The observed surface height changes show the same phase as ob-
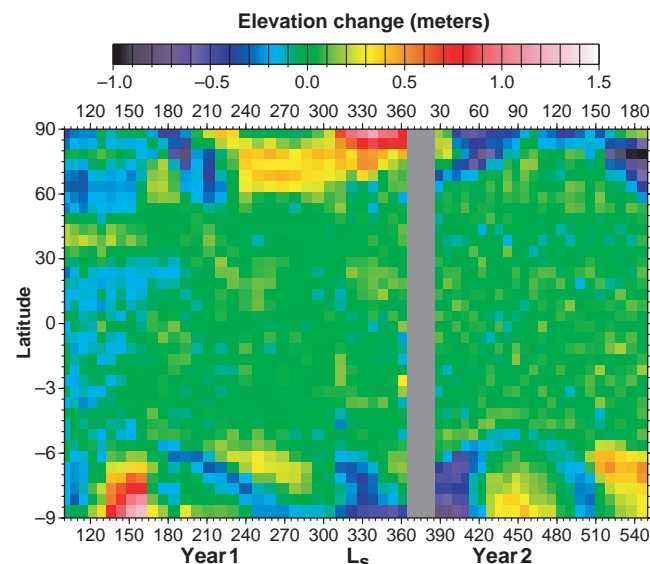
tained in the profile analysis, and at midlatitudes the amplitudes are in agreement. But the crossover analysis suggests greater peak values than obtained in the profile analysis. The difference is at least in part a consequence of the smoothing used in the profile analysis (*23*) and also of the way in which systematic errors affect the two methods. We view the difference between the two as a measure of the possible error in the magnitude of either estimate.

Most of the temporal trends (Figs. 3 and 4) are consistent with GCM simulations of the expected phase of deposition or sublimation (Web fig. 4) (*2*) and of precipitated CO_2, although the observed pattern is more complicated. However, there is an important aspect of the observed martian snow distribu-

tion that is not predicted in simulations. In both the northern and southern hemispheres, but particularly in the south, we observed transient accumulation, presumably of CO_2, in the summer. Figure 4 shows ~40 cm accumulated in the north near the end of the summer ($L_s \sim 540°$, latitude = 85°N) and 30 and 50 cm accumulated in late spring/early summer in both Mars years ($L_s \sim 250°$ and $L_s = 520°$ to 547°, both at latitude = 65°S). In the north, summer snow was observed only on the residual ice cap, whereas in the south the accumulation was observed off the residual cap. Models of the martian CO_2 cycle show that condensation from the gaseous to the solid phase occurs when the temperature drops below the CO_2 condensation point (*28*). In such models, temperature is sensitive

Fig. 4. Temporal distribution of elevation change on Mars from MOLA crossovers. Crossover residuals are averaged over 15-day intervals, plotted as a function of latitude and L_s. Cooler hues denote regions with lower than average topography, whereas warmer hues denote higher than average topography. The gray zone corresponds to a data gap around Mars solar conjunction (*18*). A discontinuity at $L_s = 163°$ in year 1 reflects a one-time change in threshold on MOLA's first trigger channel (*42*).

Fig. 3. Minimum and maximum elevation changes in the northern (blue) and southern (red) hemispheres as a function of latitude over the course of a martian year. The black arrow shows the southernmost extent of the north polar residual ice cap. On the north polar cap, the accumulation is greater than expected from the quasi-linear latitudinal trend that characterizes both hemispheres equatorward of 80°.

Table 1. Estimated geodetic and geophysical parameters.

Parameter	Value
*GM** and Love number	
GM, Mars (kg m^3 s^{-2})	4282371.6 ± 0.2 × 10^6
GM, Phobos (kg m^3 s^{-2})	0.71 ± 0.2 × 10^6
Love number k_2	0.055 ± 0.008
Maximum height of seasonal cap	
North (m)	1.5 ± 0.25
South (m)	0.9 ± 0.30
Mass of seasonal cap (latitude 60°–86°)	
North (kg)	3.1 × 10^{15}
South (kg)	3.3 × 10^{15}
Height precision of mean of annulus	
North (m)	±0.06
South (m)	±0.05
Density of seasonal deposits	
Temporal average (kg m^{-3})	910 ± 230
Gravity change of seasonal cap	
$\Delta C_{2,0}$, northern hemisphere (from altimetry†)	1.94 × 10^{-9}
$\Delta C_{2,0}$, southern hemisphere (from altimetry†)	1.98 × 10^{-9}
$\Delta C_{2,0}$, semiannual period (from tracking†)	1.96 ± 0.69 × 10^{-9}
$\Delta C_{2,0}$, semiannual period (from GCM*)	1.84 ± 0.38 × 10^{-9}

*Product of universal gravitational constant G and planetary mass M.   †Values quoted are peak-to-peak variations, which are equivalent to twice the amplitude for sinusoidal signals.

to insolation, polar cap emissivity and albedo, and atmospheric dynamics (29). Off-season accumulation is unexpected and could potentially involve shadowing of the surface by regional topography, wind-related redistribution of surface frost, or transient local storms with intensities greater than predicted by current global-scale dynamics models.

GCMs that simulate the cycle of CO_2 exchange (27, 30, 31) do not calculate the thickness of surface deposits but rather atmospheric pressure changes and condensed and sublimated mass. Figure 5 shows the semiannual pattern of precipitated mass derived from the profile data for a full martian year (32). The figure demonstrates the repeatability of the total implied mass exchange cycle based on altimetric observations collected one martian year apart. But although the global cycle is repeatable, there is regional variability because not all latitudes repeat exactly.

The global-scale mass redistribution implied by observed surface elevation changes suggests that the yearly cycle of CO_2 exchange should also produce changes in the martian gravity field. Of note is the planetary flattening, which measures the relative distribution of mass in equatorial versus polar regions and corresponds to the $C_{2,0}$ term of the gravity field. Simulations suggest that the flattening should vary by about 1 part in 10^9 because of the seasonal movement of CO_2 (32, 33). The flattening of Mars decreases as atmospheric CO_2 condenses at high latitudes and increases as polar surface deposits sublime into the atmosphere and presumably redistribute globally via sublimation winds and the Hadley circulation (34).

From MGS tracking data, we have recovered (35) the temporal variation of the $C_{2,0}$ gravity field coefficient (Table 1). Although the change in $C_{2,0}$ due to the cycle of CO_2 exchange is expected to display a quasi–

semi-annual variation because of the alternating pattern of deposition and sublimation in the northern and southern hemispheres (32), in practice the recovered signal (Fig. 6A) contains contributions from several other zonal gravity coefficients (such as $C_{1,0}$, $C_{3,0}$, and $C_{4,0}$), all of which can have observable signals but are largely inseparable (36). The observed gravity and altimetry exhibit the phase predicted by the GCM (Fig. 6B). In the determination of mass from elevation change, we chose a density of 1000 kg m^{-3} to approximately match the amplitude of the observed temporal gravity signal.

The latitudinal distribution of deposited mass in the northern and southern hemispheres (Web fig. 5) (2) indicates that (i) a larger mass is deposited on the northern ice cap relative to the comparable area of southern layered deposits, (ii) equal deposition occurs in both hemispheres between latitudes of 70° and 80°, and (iii) there is greater deposition in the south than the north at latitudes below 70°. The trend at latitudes 60° north and south in Web fig. 5 (2) and the variation in the minimum elevation (Fig. 4) indicate that our choice of the 60° latitude cutoff (20) in the measurement of elevation changes could result in an underestimation of 5 to 10 cm in the amplitude of the seasonal signal (23). Extrapolation to lower latitudes of the mass variation shown in Web fig. 5 (2) suggests that deposition may reach latitude 55° in the northern hemisphere and 50° in the south. Further, as a result of not including deposition below latitudes 60°, we may have underestimated the condensed mass by about 2.5% in the north and about 8.1% in the south.

We can use the general agreement between the altimetry-inferred changes in $C_{2,0}$, the observed changes in $C_{2,0}$ from the tracking data, and the computed changes in $C_{2,0}$ from the GCM (Fig. 6 and Table 1) to derive estimates of the density of the deposited material (37). Our estimate of the upper limit in density is 910 ± 230 kg m^{-3}, which is close to the density of water ice but is 43% less dense than CO_2 ice (38). Because our analysis of the altimetry may have underestimated the dynamic range of elevation change (23), the density probably represents an upper limit.

The results suggest that on a spatially and seasonally averaged basis and within the limits of uncertainty, condensed CO_2 deposits on Mars are more dense than terrestrial snow or compacted snowpacks, despite the lower gravitational attraction on Mars than on Earth. The results are consistent with a denser CO_2 composition and with thermal emission observations of widespread surface condensation and the hypothesized presence of slab ice in certain areas (39–41), but the current analysis cannot distinguish spatial variations
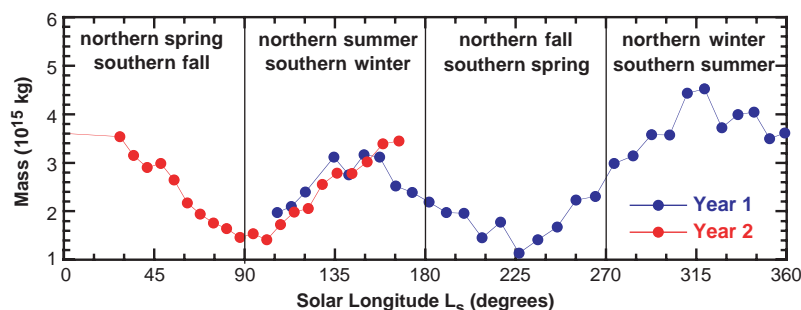
Fig. 5. Condensed CO_2 mass inferred from seasonal elevation changes of MOLA topography, assuming a density of condensed material of 1000 kg m^{-3}. MGS mapping began at $L_s = 103°$, and results are shown for more than one martian year to demonstrate the repeatability of the cycle of mass exchange. The peaks in surface mass are observed in late winter in each hemisphere.
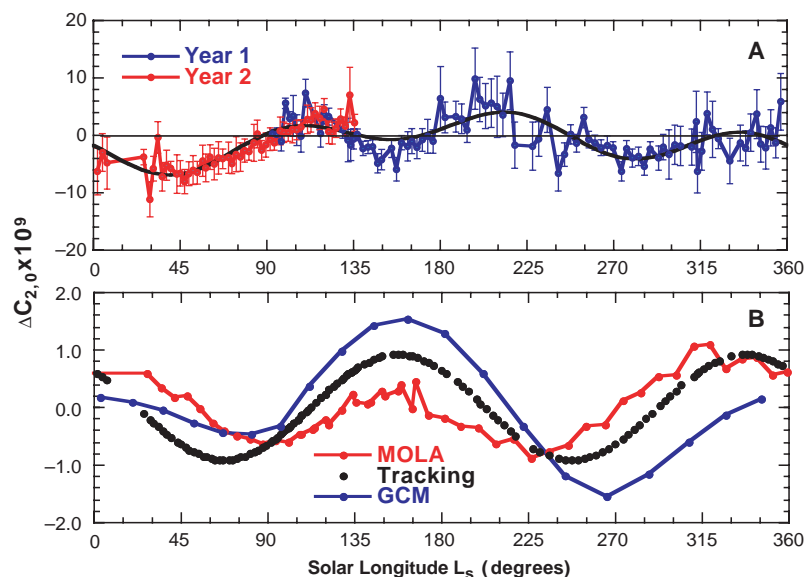
Fig. 6. (**A**) Observed seasonal variation of the planetary flattening ($C_{2,0}$ gravity field term), along with a fit (black line) consisting of annual, semiannual, and triannual terms (36). (**B**) Semiannual component of the observed $C_{2,0}$ gravity variation, the value predicted from observed MOLA elevation changes, and the value from a GCM simulation of a typical seasonal cycle of CO_2 exchange (32).

in surficial density.

Our estimate of the seasonal variation in $C_{2,0}$ from the tracking data is slightly larger than the GCM-predicted variation and could be ascribed to non-CO_2 material, such as dust, being deposited with the CO_2 on the surface. If so, it would suggest that approximately $(10 \pm 40)\%$ of the deposited mass is dust. Because this material is likely to have a density about twice that of CO_2 ice, its impact on the estimated density of the CO_2 will be a reduction of 3 to 5%.

References and Notes

1. R. B. Leighton, B. C. Murray, *Science* **153**, 136 (1966).
2. Supplementary Web material is available on *Science* Online at www.sciencemag.org/cgi/content/full/294/5549/2141/DC1.
3. P. B. James, H. H. Kieffer, D. A. Paige, in *Mars*, H. H. Kieffer, B. M. Jakosky, C. W. Snyder, M. S. Matthews, Eds. (Univ. of Arizona Press, Tucson, AZ, 1992), pp. 934–968.
4. D. E. Smith, M. T. Zuber, *Science* **271**, 184 (1996).
5. D. E. Smith *et al.*, *Science* **284**, 1495 (1999).
6. C. B. Farmer, D. W. Davies, D. D. LaPorte, *Science* **194**, 1339 (1976).
7. H. H. Kieffer, S. C. J. Chase, T. Z. Martin, E. D. Miner, F. D. Palluconi, *Science* **194**, 1341 (1976).
8. H. H. Kieffer, *J. Geophys. Res.* **84**, 8263 (1979).
9. E. S. Barker, R. A. Schorn, A. Woszczyk, R. G. Tull, S. J. Little, *Science* **170**, 1308 (1970).
10. B. M. Jakosky, E. S. Barker, *Icarus* **57**, 322 (1984).
11. B. M. Jakosky, R. M. Haberle, *J. Geophys. Res.* **95**, 1359 (1990).
12. M. T. Zuber *et al.*, *Science* **282**, 2053 (1998).
13. M. T. Zuber *et al.*, *J. Geophys. Res.* **97**, 7781 (1992).
14. A. A. Albee, R. E. Arvidson, F. Palluconi, T. Thorpe, *J. Geophys. Res.* **106**, 23291 (2001).
15. MOLA (*13*, *42*) is a 10-Hz laser ranging system that measures the round trip time of flight of 1.064-μm laser pulses between the MGS spacecraft and surface of Mars. Vector subtraction of the one-way range from the radial distance of the MGS spacecraft from Mars' center of mass as determined from the MGS Radio Science Experiment (*43*) yields measurements of the planetary radius. Radius is converted to geopotential topography by subtracting the value of the martian areoid (*44*) from each radius measurement. In the ~400-km-altitude MGS mapping orbit, the diameter of the MOLA footprint on the martian surface is ~168 m, and the shot-to-shot spacing is ~300 m. Before averaging, topography measurements have an accuracy of <1 m (Web table 1) (*2*).
16. Crossovers are locations where two spacecraft orbit tracks cross. For unchanging topography, the elevation at the crossover point should be the same in both orbit tracks, in which case the misfit provides a measure of the accuracy of the global topographic model. We corrected for twice-per-revolution orbital errors using 8,813,985 crossovers at latitudes equatorward of 57°, as well as at higher latitudes whose orbits lie within the same 15-day time interval. After orbital corrections, we examined residuals for each track at >66 million crossover locations at all latitudes, assuming the crossing track was fully corrected. We averaged these crossing errors in 15-day by 5°-latitude bins. In the average, we excluded residuals >12 m because larger residuals are presumed to represent erroneous location or sampling errors. We also excluded shot-to-shot slopes (with an ~300-m baseline) higher than 0.1. The resulting crossover residual represents the deviation from a year-round average surface elevation.
17. MGS used "two-way" Doppler radio tracking observations at 7.9 and 8.4 GHz. Measurements were averaged in 10-s intervals and have an accuracy of better than 0.1 mm s^{-1}.
18. MOLA operated continuously during the MGS primary mapping mission, with two exceptions. All MGS instruments were turned off for a 2-week period in April 1999 during spacecraft testing to assess and characterize an obstruction of the high-gain antenna. In addition, MOLA was turned off for a 2-month period in June-July 2000 surrounding solar conjunction. Near conjunction, increased plasma noise due to the close proximity of Mars to the Sun as viewed from Earth results in a degradation of the spacecraft orbit around Mars, which translates to a degradation in the accuracy of global topography measurements.
19. One day on Mars is about 24 hours and 37 min. A martian year is 687 Earth days or 668 Mars days.
20. Quoted errors are based on the statistics of the data set and do not include allowance for systematic errors, which we treated separately. For example, we corrected for a systematic range drift due to the change in the center of mass of the MGS spacecraft due to fuel consumption. In addition, we corrected for a systematic variation at all latitudes of a temporal signal with a 50-cm amplitude and a phase that matched the synodic period of Mars. To correct for this likely ephemeris error as well as for other unmodeled spacecraft orbit errors that could potentially be misinterpreted as seasonal elevation changes, we differenced elevation residuals within each annulus to the signal of a nearby latitudinal annulus that should not exhibit a seasonal signal. On the basis of extrapolation of the falloff of deposition with latitude (Fig. 3), of visual and near-infrared observations of surface frost (*3*, *40*, *45*), and of GCM simulations of the CO_2 cycle (*27*), it is likely that accumulation extends to between 50° and 60° latitude in both hemispheres. However, the temporal signal equatorward of 60° in the southern hemisphere is complicated by atmospheric effects associated with the Hellas impact basin. Thus, for consistency, we differenced the signal in each hemisphere to that at 60° latitude in that hemisphere, but extrapolated to lower latitudes to correct our estimate of condensed mass (Web fig. 5) (*2*).
21. During the mapping mission, instruments on the MGS spacecraft observed the martian surface in a nadir-pointing configuration. The orbit of MGS has an inclination of 92.7°, which results in a 5.4° gap over each pole. The spacecraft was periodically tilted to an off-nadir viewing position to collect altimetry within the gap, but these observations have greater range errors than data collected during nadir viewing because of range walk associated with spreading of the optical pulse. To minimize errors, data within the polar gaps were excluded, and the observations we report are for locations equatorward of ±87°.
22. In the profile analysis, we analyzed only MOLA channel 1 triggers (*13*, *42*) to minimize range walk errors. We calculated the median of all samples at a given latitude, sorted by longitude, within ±12 samples of point i, to use as the time-averaged baseline. We used the median of topography to define the time-averaged basal surface from which biweekly median elevations were differenced, because this measure reduced noise due to outliers associated with local topographic excursions.
23. Smoothing of the topographic data reduced the peak values of the elevation changes by 15 to 20 cm. Because the seasonal change in elevation is not a pure sinusoidal variation, it could have affected our estimates of maximum elevation. The root mean square of the original data about the smoothed data is 16 cm in the north and 18 cm in the south. We allowed 10 cm at both poles as possible underestimation errors of the maximum elevations. In addition, we estimated the minimum elevation at each latitude, which should be zero. However, Fig. 3 indicates that our average minimum is about −5 cm in the north and is zero in the south but varies nearly linearly with latitude. Although our minimum is slightly positive at high southern latitudes, it is negative at lower latitudes, which are more important in estimating condensed mass because they represent more area and volume. Consequently, we allowed an additional 5 cm in the north and south as possible underestimates of the amount of seasonal material. In estimating the density of material, we adopted a sigma of ±15% for the uncertainty of $C_{2,0}$ because it is weighted by the higher latitudes.
24. M. D. Smith, J. C. Pearl, B. J. Conrath, P. R. Christensen, *J. Geophys. Res.* **106**, 23929 (2001).
25. G. H. Pettengill, P. G. Ford, *Geophys. Res. Lett.* **27**, 609 (2000).
26. G. A. Neumann, D. E. Smith, M. T. Zuber, in preparation.
27. R. M. Haberle *et al.*, in preparation.
28. CO_2 condenses into the solid phase at a temperature of approximately 148 K at the average martian surface pressure of approximately 610 Pa.
29. D. A. Paige, S. E. Wood, *Icarus* **99**, 15 (1992).
30. R. M. Haberle *et al.*, *J. Geophys. Res.* **98**, 3093 (1993).
31. R. J. Wilson, *Geophys. Res. Lett.* **24**, 123 (1997).
32. D. E. Smith, M. T. Zuber, R. M. Haberle, D. D. Rowlands, J. R. Murphy, *J. Geophys. Res.* **104**, 1885 (1999).
33. B. F. Chao, D. P. Rubincam, *J. Geophys. Res.* **95**, 14755 (1990).
34. R. W. Zurek *et al.*, in *Mars*, H. H. Kieffer, B. M. Jakosky, C. W. Snyder, M. S. Matthews, Eds. (Univ. of Arizona Press, Tucson, AZ, 1992), pp. 835–933.
35. Time variations in gravity were recovered with the GEODYN/SOLVE orbit determination and parameter estimation software system (*46–48*). These programs numerically integrate the spacecraft cartesian state and force model partial derivatives, and include in the force modeling a spherical harmonic representation of the martian gravity field, as well as point mass representations for the Sun and other planets. The solution also includes recovery of solar radiation pressure, atmospheric drag, measurement and timing biases, and tracking station coordinates. From the orbital and tracking data, we developed normal equations that related the observation to parameters in the orbital and geophysical models, such as orbital elements, gravity coefficients, and drag parameters. From inversion of the normal equations using available tracking data, we produced low-degree spherical harmonic solutions for the gravity field of Mars and dynamical parameters, including the pole position, rotation rate, solid body tide k_2, and the mass of Phobos (*49–51*). The seasonally exchanged mass of Mars is approximately equal to the mass of Phobos; given the equatorial orbit of Phobos and the polar orbit of MGS, the spacecraft is subtly perturbed by the moon on every orbit and so solution for Phobos' mass was essential. To recover Phobos' mass, we employed the distant encounter approach demonstrated using tracking of the Viking orbiters and Mariner 9 (*52*).
36. The temporal variation of the $C_{2,0}$ gravity signal was determined in two ways. In the first, we divided the tracking data into successive 5-day arcs and inverted for a low-degree gravity field for each. The $\Delta C_{2,0}$ signal due to the seasonally induced change in the planetary flattening has a semiannual period of the form $\cos(2L_s)$, but in practice the recovered coefficient contains additional contributions. To isolate the change in planetary flattening, we fit the observed change in $C_{2,0}$ to the first three terms in a Fourier series of the form $A_n \cos(L_s + \phi_n)$, where A_n is the amplitude and ϕ_n is the phase. The $n = 1$ term is the annual period and is due to spectral leakage from power in the $C_{1,0}$ and $C_{3,0}$ gravity coefficients, which measure the offset of the center of mass of Mars from the center of figure due to the movement of CO_2 from one pole to the other. The amplitude of this signal corresponds to ~5 cm in the areoid (*32*). The $n = 2$ term is the signal of interest. The $n = 3$ term is the sink for unmodeled perturbations in the parameter recovery. In the second approach, we estimated from the yearly solution periodic variations in $C_{2,0}$ with seasonal frequencies, solving for the linear rate and the amplitudes of cosine and sine terms. Although the variations in low-degree gravity changes are not strictly periodic because of the different contributions from the two hemispheres (*32*), this approach nonetheless verified the amplitude and phase of the $n = 2$ term obtained with the first recovery method.
37. A comparison of the amplitude of $\Delta C_{2,0}$ from altimetry (0.987×10^{-9}) and tracking (0.953×10^{-9}) yields a ratio of 0.974. Because the altimetry assumed $\rho = 1000$ kg m^{-3}, the implied density is 974 kg m^{-3}. The GCM predicts a variation of $C_{2,0}$ (*32*) with average amplitude 0.85×10^{-9}. Comparison with the value derived from altimetry yields a ratio of 0.94 and a density of 873 kg m^{-3}. In computing the weighted mean density of 910 ± 230 kg m^{-3}, we assumed errors in $C_{2,0}$ of 15% in the altimetry, 36% in the tracking, and 27% in the GCM.

38. The density of CO_2 ice is 1589 kg m^{-3} at 180 K (*53*). By correcting for expected compaction given martian gravity, the density of deposited CO_2 could in principle be calculated (*54*) if the depth distribution of the crystal sizes is known. However, the distribution of CO_2 crystal sizes on Mars is not well known (*39*). On Earth, powdery snow has a density of 30 to 100 kg m^{-3}, whereas a typical winter snowpack has a density of 300 kg m^{-3}.

39. H. H. Kieffer, T. N. Titus, K. F. Mullins, P. R. Christensen, *J. Geophys. Res.* **105**, 9653 (2000).

40. T. N. Titus, H. H. Kieffer, K. F. Mullins, P. R. Christensen, *J. Geophys. Res.* **106**, 23181 (2001).

41. The southern polar region displays a puzzling, spatially variable, thermal emission signature (*39*), with some areas exhibiting a combination of low temperatures and low albedo. These physical characteristics have been interpreted as evidence for "slab ice" (*40, 55*): frozen, transparent CO_2 deposits on the surface that reveal low-albedo terrain beneath.

42. D. E. Smith *et al.*, *J. Geophys. Res.* **106**, 2689 (2001).

43. G. L. Tyler *et al.*, *J. Geophys. Res.* **106**, 23327 (2001).

44. F. G. Lemoine *et al.*, *J. Geophys. Res.* **106**, 23359 (2001).

45. X. Sun, J. B. Abshire, G. A. Neumann, M. T. Zuber, *Eos* **82**, P42A-557 (2001).

46. D. D. Rowlands *et al.*, *GEODYN II System Description* [Hughes/STX Contractor Report, Lanham, MD, 1993].

47. J. J. McCarthy *et al.*, *GEODYN Systems Descriptions and Operations Manuals* (NASA/Goddard Space Flight Center and Hughes/STX Contractor Report, Lanham, MD, 1994).

48. D. E. Pavlis, S. G. Poulouse, S. C. Rowton, J. J. McCarthy, *GEODYN Operations Manuals* (Raytheon Information Technology and Scientific Services Contractor Report, Lanham, MD, 2001).

49. D. E. Smith *et al.*, *J. Geophys. Res.* **98**, 20871 (1993).

50. D. E. Smith *et al.*, *Science* **286**, 94 (1999).

51. M. T. Zuber *et al.*, *Science* **287**, 1788 (2000).

52. D. E. Smith, F. G. Lemoine, M. T. Zuber, *Geophys. Res. Lett.* **22**, 2171 (1995).

53. O. Maass, W. H. Barnes, *Proc. R. Soc. London Ser. A* **111**, 224 (1926).

54. J. L. Foster *et al.*, *J. Geophys. Res.* **103**, 25839 (1998).

55. H. H. Kieffer, thesis, California Institute of Technology, Pasadena, CA (1968).

56. We acknowledge contributions from the MOLA instrument team, the MGS Radio Science Team, and the MGS spacecraft and operation teams at the Jet Propulsion Laboratory and Lockheed-Martin Astronautics. We thank R. Haberle, D. Paige, and J. Wahr for detailed reviews; F. Lemoine, D. Rowlands, and S. Fricke for orbit analysis; M. Torrence, P. Dunn, and J. McCarthy for gravity analysis; O. Aharonson for altimetry analysis; and P. Christensen, J. Foster, D. Hinson, H. Kieffer, J. Pearl, M. Smith, and L. Tyler for helpful discussions. The MGS MOLA and Radio Science investigations are supported by NASA's Mars Exploration Program.

Observational Evidence for an Active Surface Reservoir of Solid Carbon Dioxide on Mars

Michael C. Malin,* Michael A. Caplinger, Scott D. Davis

High-resolution images of the south polar residual cap of Mars acquired in 1999 and 2001 show changes in the configuration of pits, intervening ridges, and isolated mounds. Escarpments have retreated 1 to 3 meters in 1 martian year, changes that are an order of magnitude larger than can be explained by the sublimation of water ice, but close to what is expected for sublimation of carbon dioxide ice. These observations support a 35-year-old conjecture that Mars has a large surface reservoir of solid carbon dioxide. The erosion implies that this reservoir is not in equilibrium with the present environment and that global climate change is occurring on Mars.

In their seminal 1966 paper on the behavior of CO_2 and other volatiles on Mars, Leighton and Murray (*1*) deduced from a numerical thermal model that the polar caps are composed of frozen CO_2. They drew three other important conclusions from this analysis: (i) The year-round presence of solid CO_2 regulates the pressure of the atmosphere. (ii) The atmospheric pressure changes cyclically on a semiannual basis because of formation and retreat of the seasonal frost caps. (iii) The total amount of CO_2 on Mars could greatly exceed that presently in the atmosphere and form a large surface reservoir. In the past 35 years, many of Leighton and Murray's predictions have been verified and demonstrated by measurements taken on Mars (*2*). However, the existence of a surface reservoir of CO_2 large enough to have important implications for long-term climate and climate stability has yet to be demonstrated (*3, 4*). Here we report observations, made with the Mars Global Surveyor (MGS)/Mars Orbiter Camera (MOC), of interannual morphologic

changes in the south polar residual cap that support the argument for a climatologically important CO_2 reservoir.

The south polar residual cap exhibits morphologies unique to that location, characterized by irregular to circular pits, remnant mesas, and other landforms, interpreted to have formed by collapse and erosion (*5*). These features range from a few tens of meters to a few hundreds of meters in scale but display only a few meters of relief (*5*).

The erosion appears confined to, and highlights the layered nature of, the uppermost materials that make up the cap. The layers are relatively uniform in thickness but display a range in surface expression that appears related to their ability to erode (*6*). As few as one to as many as six layers crop out at various locations within the cap; not all layers are seen at all locales. On the basis of shadow measurements made during this investigation, each layer is about 3 m thick.

MOC was first used to observe the south polar region at high resolution in July 1999 (*7*). To search for changes, specific locations within the residual cap were reimaged at the same season and time of day beginning in late July 2001 [starting around heliocentric longitude

(L_s) 223°±4° and continuing since then]. In each case, a 2.2 to 3.7 m/pixel image covering a portion of an earlier image was acquired (*8*). Upon receipt, both the original and new images were processed for analysis (*9*).

Figure 1 shows good examples of pits, intervening ridges, and isolated mounds that have changed. Diametric measurements, made on 100 features on each of four image pairs, indicate that these pits enlarged or their intervening ridges shrank by about 6 ± 2 m and features smaller than ~6 m across disappeared. In other words, in these examples, nonhorizontal surfaces appear to have retreated by ~3 m. Other areas within the residual cap display different morphologies, and some of these show no detectable change. Preliminary statistics suggest that between 25 and 50% of the escarpments have retreated between 1 and 3 m.

As part of the input to an estimate of the total amount of scarp retreat that occurred during the past martian year, the total perimeter in a variety of settings was determined by image processing techniques (*10*) and divided by the area viewed. Measurements were made on images representative of the range in areal density of various forms of escarpments within the residual south polar cap. The average scarp perimeter per area was 2.4×10^{-2} m/m^{-2}.

We determined that the amount of retreat was consistent with the subliming of a volatile ice by calculating the annual solar insolation using software based on spacecraft navigation routines, and we compared our results with the results of previous models of polar cap behavior (*1, 11–13, 14*). We used the order of magnitude greater volatility of CO_2 relative to water ice to differentiate between these two candidates. Table 1 summarizes the results of our calculations of the insolation and the equivalent areal mass density for H_2O and CO_2 ice for horizontal surfaces at various latitudes from the equator to near the south pole.

A variety of factors affect the translation of the maximum equivalent areal mass loss (Table

Malin Space Science Systems, Post Office Box 910148, San Diego, CA 92191–0148, USA.

*To whom correspondence should be addressed.